Nonmonotonous temperature fluctuations of the orbital moment and spin-orbit coupling in multiferroic gallium ferrite thin films

Benjamin Meunier,[1] Suvidyakumar Homkar,[1] Fadi Choueikani,[2] Mathieu G. Silly,[3] Christophe Lefèvre,[1] François Roulland,[1] Cédric Leuvrey,[1] Jérôme Robert,[1] Daniele Preziosi,[1] and Nathalie Viart[1]

[1]*Université de Strasbourg, CNRS, IPCMS, UMR 7504, F-67000 Strasbourg, France*

[2]*DEIMOS Beamline, Synchrotron SOLEIL, L'Orme des Merisiers, Départementale 128, 91190 Saint-Aubin, France*

[3]*TEMPO Beamline, Synchrotron SOLEIL, L'Orme des Merisiers, Départementale 128, 91190 Saint-Aubin, France*

(Received 10 March 2022; revised 26 August 2022; accepted 19 October 2022; published 10 November 2022)

Temperature dependent x-ray absorption spectroscopy and x-ray magnetic circular dichroism experiments were performed at the Fe $L_{2,3}$ edges to unveil the magnetic orbital moment and spin-orbit coupling (SOC) behavior in thin films of the multiferroic $Ga_{0.6}Fe_{1.4}O_3$ (GFO) compound. A thorough analysis of the data evidenced a nonmonotonous behavior for both magnetic orbital moment and SOC with a minimum at approximately 120 K, accompanied with indications of disturbances of the magnetic exchange and electric field dipole. Resonant photoemission spectroscopy experiments performed at the Fe $L_{2,3}$ edges rendered an important modification of the crystal field configuration around this temperature value, pointing to a temperature-driven structural trigonal distortion. These instabilities can be compared to those observed in other iron oxides, in particular, during transitions such as the Verwey transition, with the difference that on GFO they do not have any impact on the macroscopic magnetic properties, such as the coercive field and the global magnetization. This work demonstrates that the absence of instabilities in magnetism at the macroscopic scale does not guarantee the absence of fluctuations at the atomic scale. Such atomic-scale fluctuations of the SOC are undoubtedly shown here and have an impact on the spin Hall magnetoresistance response of the films. This point is of importance for prospective applications of GFO in spin-orbitronics.

DOI: 10.1103/PhysRevB.106.184410

I. INTRODUCTION

Transition metal oxides (TMOs), with their numerous and interconnected degrees of freedom, are at the heart of great expectations in the context of ever increasing needs of speed and density for electronic devices [1], and are, in that context, importantly cited in electronics roadmaps [2–4]. Among the most promising TMOs, one finds the magnetoelectric multiferroic ones, in which the intertwining of the magnetic and electric properties opens opportunities for low energy manipulation of magnetic properties by an electric field in spintronic devices [5]. New paradigms involving spin-orbit coupling (SOC) have recently been proposed to further enhance the logic performance of the devices [6]. SOC in TMOs is definitely perceived as the ultimate tool for new spintronics strategies based upon charge and spin interconversion processes [7]. Unveiling how SOC operates in multiferroic TMOs is essential to its exploitation in future ultralow switching energy spintronic devices.

A strong orbital-lattice interaction was recently evidenced in the room temperature magnetoelectric multiferroic gallium ferrite $Ga_{1-x}Fe_xO_3$ (GFOx) with a nonzero magnetic orbital moment (m_L) unexpectedly opposite to the spin one [8]. GFOx crystallizes in the orthorhombic $Pc2_1n$ (33) space group and the cations are distributed over four different cationic sites, the tetrahedral Ga1 and the three octahedral, Ga2, Fe1, and Fe2. Magnetism in this compound results from antiferromagnetic superexchange interactions between the Fe^{3+} cations in the four nonequivalent sites [9,10], which globally yield an antiparallel ordering between the (Ga1, Fe1) and (Ga2, Fe2) sites. In such a competition context, slight modifications of the Fe-O-Fe exchange pathways, in either angles or distances, can induce important modifications of the exchange interactions. Temperature dependent structural instabilities were indeed observed to induce important modifications of the orbital moment for Ga-free isostructural compound ε-Fe_2O_3 (EFO) [11], in the form of a strong reduction of m_L around 110 K. This atomic-level feature was accompanied with changes in the macroscopic magnetic measurements, in the form of the collapse of the coercivity [12,13]. Since GFOx presents a much higher resulting magnetization (ca. 100 emu/cm^3 at room temperature for GFO1.4) [14] than the almost completely compensated antiferromagnet EFO, the investigation of the temperature behavior of its orbital moment and SOC are of high interest with regard to applications.

Here, we report a temperature study of the magnetic orbital moment and SOC in $Ga_{0.6}Fe_{1.4}O_3$ (GFO1.4) thin films through temperature dependent x-ray absorption spectroscopy (XAS) and x-ray magnetic circular dichroism (XMCD) experiments performed in normal incidence at the Fe $L_{2,3}$ edges. The orbital and spin moments were determined from the XMCD data using the sum rules [15,16]. We show that, despite the absence of any macroscopic signature such as a

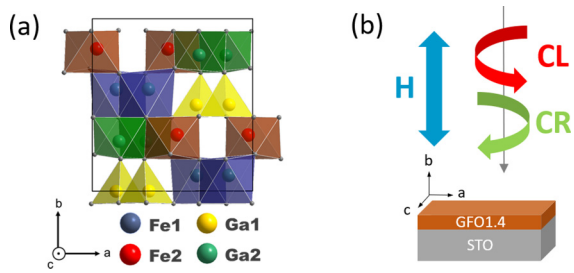

FIG. 1. (a) $Pc2_1n$ structure of GFO with the four different cationic sites. (b) Experimental configuration used for the XAS and XMCD measurements.

collapse of the coercivity, m_L does present a minimum value at 120 K, as well as the spin-orbit coupling. Resonant photoemission spectroscopy (RESPES) was used to get further details in the electronic structure at the Fe $L_{2,3}$ edges. It allowed evidencing changes in the crystal field configuration with temperature, with an important increase of the trigonal distortion of the Fe octahedra for temperatures above 140 K. The system thus shows signatures of a transition driven by spin-orbital-lattice interactions, emblematic of highly correlated systems.

II. EXPERIMENTAL DETAILS

We studied 64 nm thick GFO1.4 thin films epitaxially grown onto (111) oriented $SrTiO_3$ (STO) single crystals by pulsed-laser deposition. Details on the growth conditions and structural characterizations are reported in Ref. [17]. The deposited GFO1.4 thin films crystallize in the $Pc2_1n$ space group, with the b axis normal to the sample surface [Fig. 1(a)] and they are fully relaxed. Soft XAS and XMCD spectra were acquired at the $Fe_{2,3}$ edge on the DEIMOS beamline of the French Synchrotron Facility SOLEIL in normal incidence geometry and in total electron yield mode with an energy resolution of ca. 0.15 eV, at temperatures varying in the 20–300 K range. Each XAS and XMCD spectrum results from the average of 16 absorption spectra alternating opposite magnetic field directions ($H = \pm 6.5$ T) and photon helicities (left/right) [Fig. 1(b)]. The magnetic field was applied perpendicular to the sample surface, i.e., along the b axis of the GFO lattice. The magnetic properties of the films were also studied with a superconducting quantum interference device vibrating sample magnetometer (SQUID VSM MPMS 3, Quantum Design) in the perpendicular configuration (magnetic field along the b axis). Hysteresis loops were measured for magnetic fields up to 7 T, in the 20–300 K temperature range.

RESPES experiments were performed at the soft x-ray TEMPO beamline of the French Synchrotron Facility SOLEIL [18]. Linearly polarized light was delivered by an HU44 Apple II undulator installed in a medium straight section of the storage ring. Resonant valence band photoemission spectra were measured using a MBS A-1 photoelectron analyzer. The instrumental work function was calibrated using the Au $4f_{7/2}$ line and the Fermi level of a clean gold surface. Simultaneously to the RESPES measurements, the drain sample current was recorded and normalized to a gold mesh signal to provide x-ray absorption spectra. The studied films were unmounted from the deposition sample holder in air and quickly placed in a vessel under primary vacuum for transport.

III. RESULTS AND DISCUSSION

Figure 2 shows the GFO Fe $L_{2,3}$ edges XAS and XMCD spectra recorded at three different temperatures, 20, 120, and 200 K. The total XAS spectra were obtained by averaging the absorption for left and right circularly polarized light and corrected from saturation effects [19] following the procedure described in detail in [8] for similar films. The XAS and

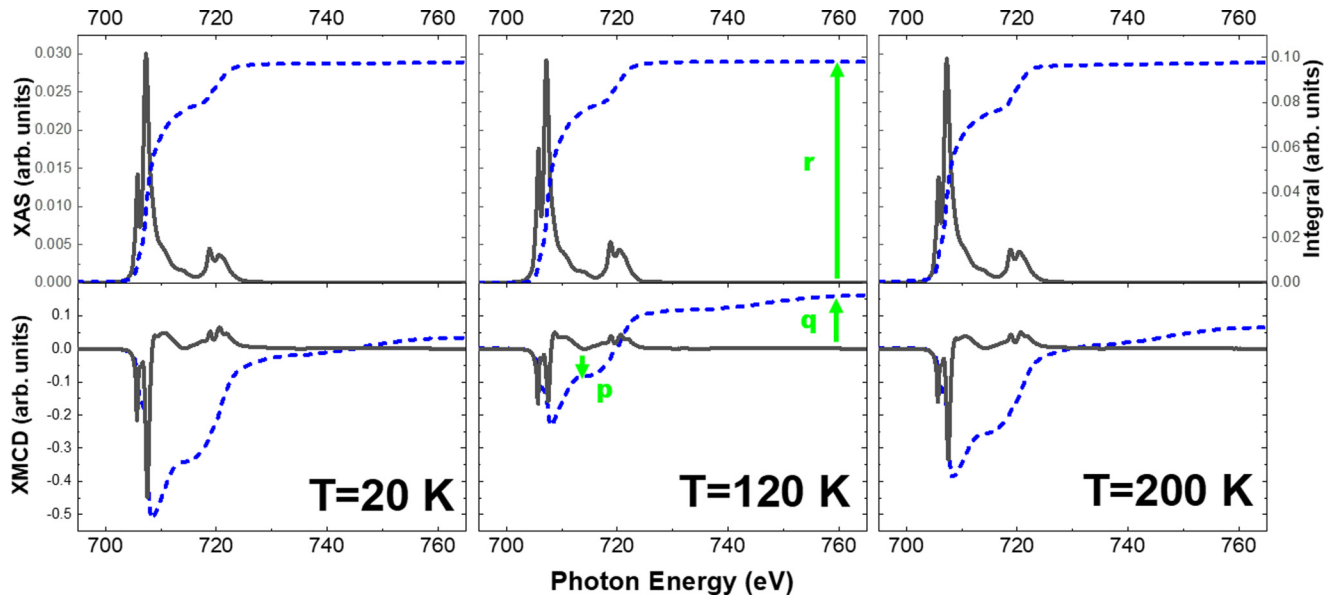

FIG. 2. Fe $L_{2,3}$ edges total XAS and XMCD spectra of a 64 nm thick $Ga_{0.6}Fe_{1.4}O_3$ film at 20, 120, and 200 K under a field of 6.5 T applied along the GFO b axis. Dotted lines (blue) correspond to the signal integration used for the sum-rule calculations. The XAS spectra have been processed by subtracting a step function as described in Ref. [15].

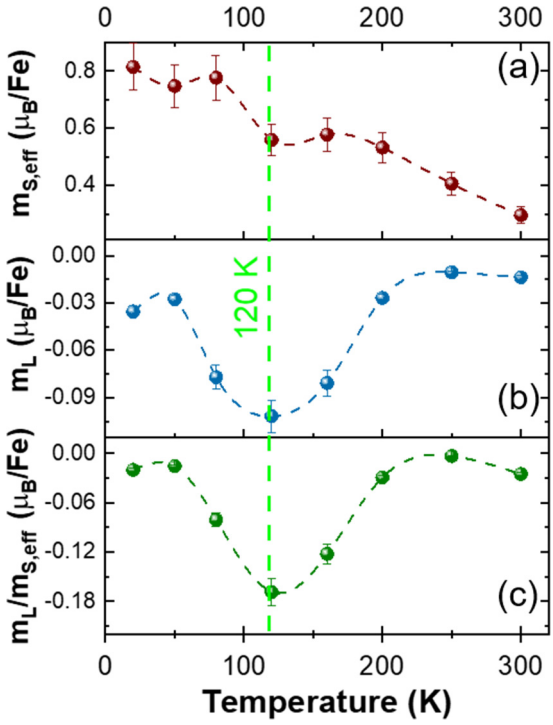

FIG. 3. Temperature dependence of (a) the effective spin moment $m_{S,\text{eff}} = m_S + m_D$, (b) the orbital moment m_L, and (c) the $m_L/m_{S,\text{eff}}$ ratio.

XMCD spectra show features associated with Fe^{3+} in an octahedral environment, with no evidence of either Fe^{2+} or Fe^{4+} (see calculation in Fig. S1 of the Supplemental Material [20]). The XMCD spectra show important variations with temperature, especially when considering the two negative peaks of the L_3 edge (at 705.7 and 707.5 eV), which are commonly ascribed to O_h sites [21]. The intensity ratio between these two peaks at the L_3 edge is about 2 for $T = 20$ and 200 K, while it is only about 1 for $T = 120$ K, pointing to a nonmonotonous temperature dependence of the GFO1.4 magnetic properties.

By using the sum rules [15], we could determine the magnetic orbital moment m_L and the effective magnetic spin moment $m_{S,\text{eff}} = m_S + m_D$, m_S being the isotropic spin moment and m_D reflecting the quadrupole contributions of the spin distribution in the atomic sphere [22]. The use of sum rules is usually restricted to materials for which the magnetic ions are in one single valence state and geometrical environment. Typically, GFO, with its four cationic sites and, more importantly, with its two different coordination and symmetry T_d and O_h sites (see the GFO structure in Fig. 1), is not the archetypal case for the use of the sum rules. However, despite the presence of a non-negligible amount of Fe cations in a T_d environment (10% of the total Fe cations; see the cationic distribution given in Table S1 in the Supplemental Material [20]) [23], no significant contribution to the overall XMCD signal is expected, because no distortion is accompanying such Td sites, unlike for the much more distorted O_h sites. Finally, one can still confidently apply the sum rules as already done in Ref. [8] for GFO thin films and Ref. [11] for ε-Fe_2O_3 (EFO, which is isostructural to GFO) nanoparticles. Figures 3(a) and 3(b) show the temperature dependence of m_L and $m_{S,\text{eff}}$. For the application of the sum rules we used the nominal number of holes ($n = 5$) expected for Fe^{3+} ions in a $3d^5$ configuration, without taking into account possible Fe-O charge-transfer effects. The effective spin moment, $m_{S,\text{eff}}$, decreases with increasing temperatures in a ferromagnetic-like behavior [Fig. 3(a)], with a slight anomaly around 120 K which is concomitant to a large minimum observed for the orbital magnetic moment, m_L [Fig. 3(b)]. One may be surprised by the nonzero value observed for m_L in such a $3d^5$ high spin system, and by the fact that it is largely negative. The origin of this negative orbital moment in $Ga_{0.4}Fe_{1.6}O_3$ thin films has been addressed in a previous study [8]. In this structure, both the orbital and spin moments result from a sum of contributions of the four cationic sites. The orbital moment originates from off-centerings of the Fe^{3+} cations in their polyhedral site and is dominated by the contribution from the most distorted Fe1 site [24–26]. The spin moment results from the antiferromagnetic alignment between the spins of the Fe^{3+} cations in the (Fe1, Ga1) and (Fe2, Ga2) sites. Due to unbalanced occupation of the cationic sites in GFO1.4 (Ga1 is mostly occupied with Ga), the resulting spin moment is imposed by the (Fe2, Ga2) component. The resulting orbital moment, being related to the Fe1 site, will thus be opposed to this resulting spin moment, and this explains the negative sign of m_L. In Fig. 3(c) we also show the $m_L/m_{S,\text{eff}}$ ratio as a function of the temperature which holds the same behavior as m_L, offering a clear indication that Fe-O charge-transfer effects, which are expected to modulate the number of holes in the $3d$ orbitals, do not play a major role in the mechanism underneath the origin of the m_L minimum. This temperature dependence of m_L is also observed for GFO1.4 thin films grown with different thickness values as shown in Fig. S2 of the Supplemental Material [20].

We have sought to extract some quantitative information from our XAS data and have resorted to the so-called branching ratio (BR). The XAS spectra show well separated L_2 and L_3 edges (Fig. 2), with an area ratio L_2:L_3 globally close to 1:5 instead of the 1:2 expected for $3d$ elements. Thole and Van der Laan have established that such a nonstatistical ratio was related to the existence of SOC [27,28]. The BR, as defined in Eq. (2), established for p to d transitions, is related to both SOC and occupancy of the $3d$ shell (p 84 of Ref. [29]):

$$\text{BR} = \frac{\int L_3 - 2\int L_2}{\int L_3 + \int L_2} = \frac{\sum_i \langle l_i s_i \rangle}{\underline{n}}, \tag{1}$$

where $\underline{n}$ is the number of holes in the $3d$ shell, and l_i and s_i are the orbital and spin angular momenta in the shell for each of the i $3d$ electrons, respectively.

Figure 4 shows the temperature dependence of the branching ratio, calculated from the experimental L_2 and L_3 areas. A minimum is observed at 120 K, mimicking the temperature dependence reported for the $m_L/m_{S,\text{eff}}$ ratio. There are very few works in the literature reporting the temperature evolution of the branching ratio for a transition metal. They mostly report a decrease of the BR with increasing temperatures (p. 84 of Refs. [29]; also see [30]) and we have not read of such a nonmonotonous behavior.

According to Eq. (2), the minimum observed at 120 K could be attributed to either a decrease of the $\sum_i \langle l_i s_i \rangle$ term,

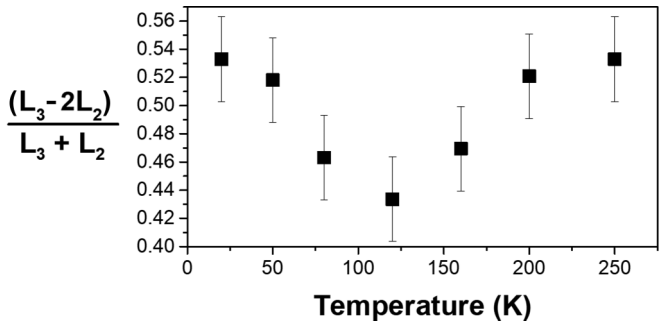

FIG. 4. Temperature dependence of the branching ratio.

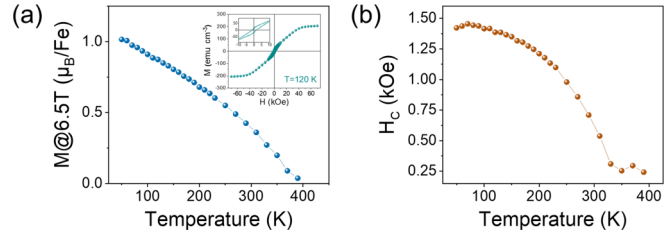

FIG. 6. Temperature evolution of (a) the magnetization of the sample at 6.5 T—the hysteresis cycle measured at 120 K is shown in the inset as representative of all measured cycles. (b) The coercive field, as measured on the hysteresis cycles performed for the different temperatures (the measurements are performed in normal geometry).

or to an increase of the number of holes (for instance, by modifying the amplitude of the O $2p$ to Fe $3d$ charge transfer). In the case where only a variation of $\underline{n}$ is considered, this would imply that Fe^{3+} is fully reduced to Fe^{2+}, which is unlikely regarding the absence of Fe^{2+} fingerprint in the XAS spectra (Fig. S1 [20]). The minimum value of the nonstatistical branching ratio thus points to a plausible modification of the spin-orbit coupling around 120 K.

Further analyzing the XAS spectra, one can notice that their double-peak line profiles at both L_3 and L_2 edges vary with temperature as well. The evolution of the relative peaks' intensity ratio was quantitatively studied at the L_2 edge. The peaks are labeled A (718.7 eV) and B (720.4 eV) and the temperature dependence of the A/B ratio, which we will name the L_2 ratio, is plotted in Fig. 5. It shows a net change of approximately 20% at about 120 K. It has been reported in the literature that such a change in the L_2 line shape can arise from a modification of the magnetic exchange interactions. A linear relationship between the L_2 intensity ratio and the magnitude of the exchange interaction has even been shown by Alders *et al.* [31]. In our case, this would indicate an increase of the total magnitude of the exchange interaction for temperatures decreasing below 120 K.

The results obtained by XAS and XMCD all point to the existence of some magnetic transition at 120 K, similar to the one observed in the isostructural compound EFO, despite the difference in cationic site occupations.

The temperature variation of the orbital moment is indeed similar to what was reported by Tseng *et al.* for EFO nanoparticles in [11], where they also observed a minimum in the orbital moment at 120 K. The positive sign of their orbital moment is probably due to the fact that the material

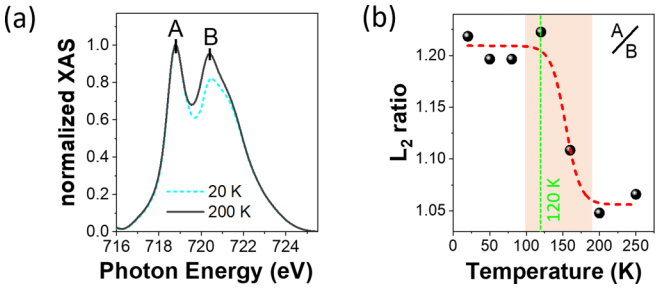

FIG. 5. (a) Closeup on the L_2 edge at 20 and 200 K. (b) Temperature evolution of the A/B ratio.

was in a disoriented polycrystalline form, and not an oriented thin film as is the case here. The orbital moment of GFO1.4 was indeed observed to be strongly anisotropic, with negative values for measurements performed in the normal incidence configuration and positive ones in grazing incidence [8]. The modification of the orbital moment observed at 120 K in EFO was ascribed to a structural instability, mainly related to modifications of the Fe-O bond lengths. In the context of the strong competition of antiferromagnetic superexchange interactions between the cationic sites in this structure, a structural instability, with Fe-O-Fe exchange path modifications, would indeed explain the instability evidenced for the exchange interaction (Fig. 5). For EFO, the bond length variations were shown to lead to an important deviation from the ideal ionic model, where Fe(O) would no longer have the nominal 3 + (2–) charge, through Fe $3d$–O $2p$ intermixing and charge transfer. This was supported by a Mössbauer study which showed important modification in the quadrupolar splitting, related to the electric field gradient, for the Fe ions in some of the cationic sites [11]. A partial charge transfer in our GFO1.4 thin film would not be detectable on the XAS spectra profile, but the anomaly at 120 K in the temperature variation of $m_{S,\mathrm{eff}}$ is certainly an indicator of such a charge related phenomenon. Indeed, the spin moment accessed by XMCD through the sum rules, $m_{S,\mathrm{eff}}$, contains an additional intra-atomic magnetic dipole moment term, m_D [32]. To be more precise, m_D is defined as $m_D^\alpha = -\frac{7\langle T_\alpha\rangle\mu_B}{\hbar}$, $(\alpha = x, y, z)$, with $\boldsymbol{T}$ the intra-atomic magnetic dipole operator, which may also be written as a coupled operator involving spin and charge components [22]. This instability of the electric field gradient at around 120 K is to be related with the strong variation in the SOC as extracted from the temperature variation of the BR (Fig. 4).

For EFO, the minimum of the orbital moment is accompanied with a collapse of the anisotropy of the material, which manifests itself as a collapse of the coercive fields. We have therefore also sought to compare the values of the spin and orbital moments of the GFO1.4 thin film determined by x-ray atomic absorption spectroscopy with the macroscopic perception one may have of the magnetism of the system from SQUID measurements. M vs H hysteresis curves were measured in the perpendicular configuration (magnetic field applied perpendicular to the film) at various temperatures ranging between 20 and 300 K for the GFO1.4 film. The inset of Fig. 6(a) shows the cycle measured at 120 K as

representative of the cycles measured for all temperatures, after the subtraction of the diamagnetic component due to the STO substrate. The temperature evolution of the magnetic moment measured at a 6.5 T magnetic field (magnetic field used for the XMCD experiments) shows a typical behavior for a ferromagnetic material, i.e., a constant decrease with increasing temperature, with no detectable anomaly at 120 K. SQUID measurements are, however, only sensitive to the monopole distribution of the spin moment m_S, while, as explained above, the spin moment accessed by XMCD through the sum rules, $m_{S,\text{eff}}$, contains an additional intra-atomic magnetic dipole moment term, m_D. This explains the difference between the two temperature evolutions. There is no anomaly present in the temperature evolution of the coercive field either [Fig. 6(b)], which also shows a constant decrease with increasing temperature. The anomaly observed for the orbital moment does not therefore seem to result in any feature for the macroscopic observations of magnetism of the compound, as is the case for EFO [12]. This might be due to the fact that the macroscopic behavior of GFO1.4 results from a less balanced competition between cationic sites, since one of them is almost entirely occupied by the nonmagnetic Ga atoms.

Despite its lack of impact on the macroscopic magnetism, the atomic-level magnetic feature is of high importance for applications in spin-orbitronics. GFO1.4 was recently proven to be a material of interest for the electric-field control of the spin current generation in nonmagnetic/ferromagnetic oxide based heterostructures through spin Hall magnetoresistance (SMR). The minimum in SOC we evidence at 120 K in the present paper was indeed shown to induce a signature in the SMR [33].

In fact, this magnetic instability observed here for GFO1.4, and which was also observed for the isostructural EFO, is certainly to be put in a broader perspective with a transition featured by another iron oxide, the Verwey transition [34] observed in a similar temperature range ($T_V = 125$ K) for the Fe_3O_4 spinel-type magnetite. The Verwey transition is described as a structural transition accompanied by a spin reorientation and a drastic modification of numerous physical properties, including spontaneous magnetization, magnetocrystalline anisotropy, and electrical conductivity [35–37]. This transition, although discovered in 1939, is still not fully understood. However, a complex charge-order pattern in relation to structural distortions inducing substantial off-center atomic displacements was recently highlighted as a possible cause [38,39]. As written earlier, no charge transfer could be experimentally evidenced by XAS for GFO1.4. We have thus undertaken a resonant photoelectron spectroscopy (RESPES) study in order to further investigate this issue and, more generally, the electronic structure of GFO1.4 and its evolution across the transition observed for the orbital moment and spin-orbit coupling. While XAS and XMCD probe the unoccupied electronic states, photoelectron spectroscopies, which are also element and site selective, probe the occupied states and are perfectly adapted to study the electronic structure of the compounds. Resonant photoemission spectroscopy (RESPES) has, for example, successfully been used to quantitatively extract the amount of the various valences present in mixed valence compounds [40] and bring information about charge-transfer processes [41]. It consists

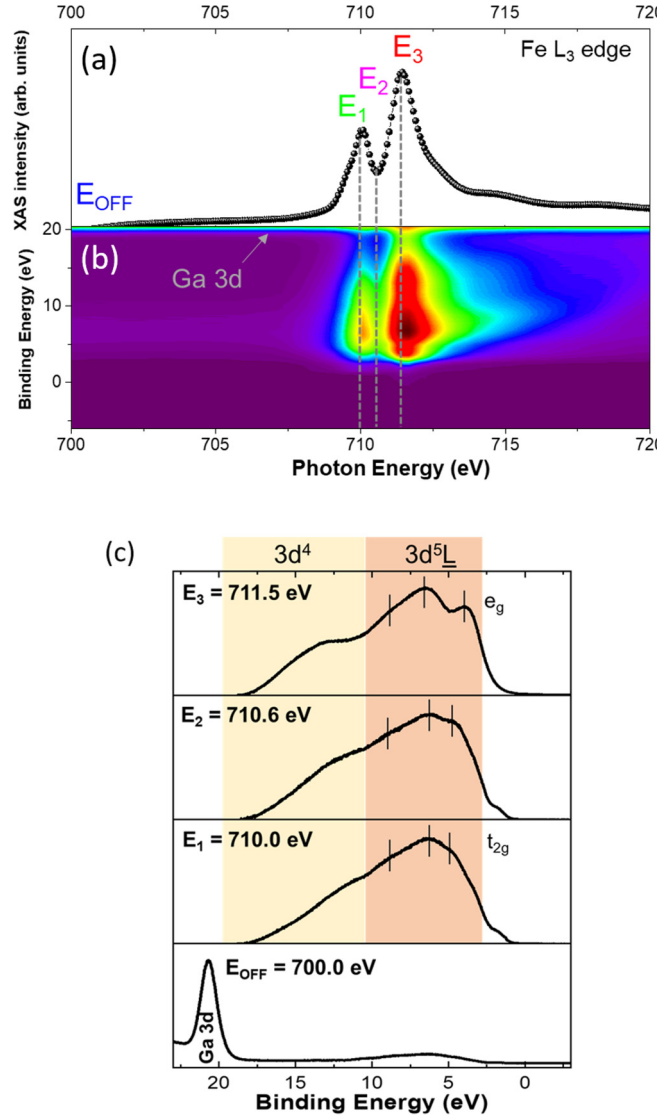

FIG. 7. (a) L_3-edge absorption spectra measured *in situ* simultaneously with (b) the corresponding L_3-edge resonant photoemission map of the GFO1.4 thin film surface, and (c) from bottom to top: off-resonance ($E_{\text{OFF}} = 700.0$ eV) valence band, with the Ga $3d$ signature, taken as the reference spectrum, and resonant photoemission spectra for three different excitation energies ($E_1 = 710.0$ eV, $E_2 = 710.6$ eV, and $E_3 = 711.5$ eV) after subtraction of the reference spectrum.

in scanning the photon energy of a soft-x ray beam in the range of a specific absorption edge and measuring the valence band spectra for these scanned energies. The advantage of this technique is to selectively enhance the valence band signal of a specific element. Here we have recorded the resonant soft x-ray $2p \rightarrow 3d$ transition of iron (Fe $L_{2,3}$ edge) on GFO1.4 thin films. A complete description of the excitation and de-excitation processes occurring in this condition is depicted in the SM (Fig. S3 [20]) [40]. One can briefly summarize them as follows: the absorption of an x-ray photon results in the transition of a core $2p$ electron to the excited valence $3d$ state [Fe $2p^6\,3d^n + h\nu \rightarrow (\text{Fe}\ 2p^5 3d^{n+1})^*$]; the relaxation and

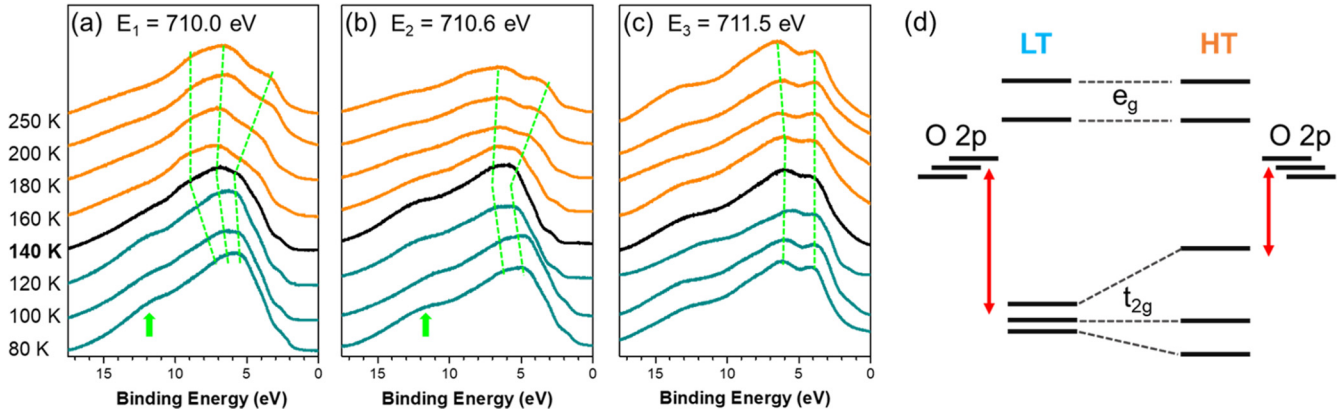

FIG. 8. Temperature dependence of the RESPES spectra for photon energies of (a) $E_1 = 710.0$ eV, (b) $E_2 = 710.6$ eV, and (c) $E_3 = 711.5$ eV—the green arrows point to the signal originating from unhybridized states. (d) Sketch of the energy diagram at low (LT $<$ 140 K) and high (HT $>$ 140 K) temperatures showing a trigonal distortion of the O_h symmetry.

autoionization of the system then occurs through the emission of an Auger electron [$(\text{Fe } 2p^5 3d^{n+1})^* \rightarrow \text{Fe } 2p^6 3d^{n-1} + e^-$].

Figure 7(a) presents the absorption spectrum measured at the Fe L_3 edge *in situ* by recording the drain current from the sample together with the resonant photoemission signal. This x-ray absorption spectrum faithfully reproduces the two main features of the L_3 edge we have already reported in our XMCD study. The resonant photoemission map simultaneously measured in the same energy range is presented in Fig. 7(b), after calibration of the binding energies on the Ga 3*d* core line (top border of the map). The raw data (before any calibration) are given in Fig. S4 of the Supplemental Material (SM) [20] and show the strong impact of the x ray absorption dependent charging effect. The two local maxima of the RESPES map perfectly match with the maxima observed for XAS. From this map, four energies of interest are selected: E_{OFF}, corresponding to the reference out of the resonance, E_1 and E_3 the two absorption maxima, and E_2 the valley in between. The detailed resonant spectra taken at these energies are shown in Fig. 7(c). The contribution from the off-resonant valence band (measured at E_{OFF}) and that of secondary electrons (using a Shirley function) have been subtracted from the three resonant spectra to remove the contribution from direct photoemission processes. The three energies correspond to three different transitions. E_1 and E_3, local maxima of the XAS spectra, are directly associated with the transitions occurring for cations in O_h sites, the lowest (E_1) being related to the $2p \rightarrow t_{2g}$ transition while the other one (E_3) corresponds to the $2p \rightarrow e_g$ transition. Calculations/simulations show that the absorption maximum from T_d symmetry is expected to arise at an intermediate energy [42]. E_2 has been chosen at the minimum of absorption between E_1 and E_3 so that the contribution from the O_h symmetry is at its lowest. One still has to remember that only 1/10 of the Fe cations are localized in T_d sites, which might not be sufficient to annihilate the domination of the signal by contributions from the O_h sites.

Figure 8 presents the temperature dependence of the RESPES spectra. At first sight, spectra recorded at E_1 and E_2 photon energies [Figs. 8(a) and 8(b), respectively] are heavily temperature dependent while those at E_3 [Fig. 8(c)] remain practically unchanged. We only notice a broadening of the E_3 spectra with temperature, possibly due to the increase of the phononic contribution at high temperature. As previously discussed, it is not surprising to find out that the signal arising from the T_d site in E_2 is mostly screened by those from O_h (both t_{2g} and e_g). E_2 will therefore not allow us to draw a conclusion regarding the temperature dependence of the T_d site. Concerning the spectra recorded at E_1, the three characteristic peaks we have previously discussed at room temperature tend to merge to form a wide single peak at low temperature. According to the multiplet theory, such a less dispersed distribution of states indicates a higher degree of symmetry of the crystal field. That information, combined with the fact that E_3 (related to e_g states) is unaffected by the temperature variation indicates that the distortion of the O_h sites is of a trigonal nature, confirming our previous observations [8], and provides the important information that the distortion varies with temperature and is smaller for lower temperatures. A sketch of the symmetry transition is shown in Fig. 8(d). The green arrows in Fig. 8 mark the signal originating from final unhybridized states, and which becomes more pronounced for temperatures lower than 140 K. This is an indication that the overlap between the O 2*p* and Fe 3*d* orbitals is lower for lower temperatures, as schematized also in Fig. 8(d).

The RESPES study thus completes the picture delineated by our temperature dependent XAS and XMCD about the modification of the electronic properties occurring in our GFO1.4 thin films. It is now clear that the modifications of the atomic-level magnetism of iron in the system, namely the minima of the orbital moment and spin-orbit coupling and variation of the magnetic stiffness, occur simultaneously with a structural distortion which induces important modifications of the symmetry of the electronic structure. These are the ingredients involved in the Verwey transition and this reinforces the parallel which can be drawn. Indeed, the Verwey transition is now understood as being due to complex relations between the electronic and structural degrees of freedom [43]. In this understanding of the phenomenon, important ingredients are the electron-phonon coupling and strong electronic correlations. In such a correlated state, the coupling between electrons and lattice enhances and stabilizes the charge-orbital order, effectively reducing the total energy. This in turn modifies the interatomic interactions and generates the anharmonic potential. This mechanism leads to the Verwey transition with

the static structural distortion and frozen charge-orbital order below T_V. In contrast, above T_V the charge-orbital degrees of freedom are dynamic and couple strongly to phonons reducing their lifetimes. In the orthorhombic $Pc2_1n$ structure of GFO and EFO, it seems that the instability does not crystallize into a complete transition and one cannot be conclusive concerning the existence of a spin reorientation in GFO1.4 since it was not evidenced by macroscopic SQUID measurements. One can still note that a kind of spin reorientation has indeed already been described in the form of a spin-glass transition in $GaFeO_3$ by Mukherjee *et al.* [44]. It is most likely that such Verwey-like instabilities are to be observed in other iron oxides at their atomic level, even if they do not result in macroscopically observable effects, provided high electronic correlation is present in the system.

IV. CONCLUSION

Temperature dependent XMCD measurements allowed the unveiling of variations of both the magnetic orbital moment and SOC in GFO1.4 thin films, with a minimum at approximately 120 K. This work presents direct monitoring of the SOC in Fe^{3+} cation based materials and observation of its nonmonotonous temperature dependence. The minimum in both m_L and SOC is accompanied with clues indicating perturbations of the magnetic exchange and electric field dipole. All this suggests similarities with the Verwey transition observed in magnetite in the same temperature range. This assumption is corroborated by a RESPES study which evidences, within the same 120–140 K temperature range, a modification of the material's electronic structure induced by a structural distortion. The absence of any macroscopic signature of the atomic-level perturbations of magnetism can be accounted for by the presence of nonmagnetic cations in some of the GFO1.4 cationic sites, which disrupt the magnetic exchange paths. The perturbations of the atomic-scale magnetism are nevertheless well present and do have an impact on the physical properties of the films as already evidenced in the applicationwise interesting spin Hall magnetoresistance response of the films.

ACKNOWLEDGMENTS

This work was funded by the French National Research Agency (ANR) through Grant No. ANR-18-CE24-0008 "ANR MISSION" and, within the Interdisciplinary Thematic Institute QMat, as part of Program No. ITI 2021 2028 of the University of Strasbourg, CNRS, and Inserm. It was supported by IdEx Unistra (Grant No. ANR 10 IDEX 0002), and by the SFRI STRAT'US projects (Grant No. ANR 20 SFRI 0012) and Grants No. ANR-11-LABX-0058_NIE and No. ANR-17-EURE-0024 under the framework of the French Investments for the Future Program. The authors wish to thank Marti Gich (Institut de Ciència de Materials de Barcelona–CSIC) for fruitful discussions. They acknowledge experimental support from the XRD, MEB-CRO, and TEM platforms of the IPCMS. The synchrotron experiments were performed at the DEIMOS and TEMPO beamlines of the French Synchrotron Facility SOLEIL. The authors are grateful to Edwige Otero and Philippe Ohresser for their scientific and technical support on the DEIMOS beamline.

B.M. and S.H. contributed equally to this work.

[1] D. C. Vaz, A. Barthélémy, and M. Bibes, Oxide spin-orbitronics: New routes towards low-power electrical control of magnetization in oxide heterostructures, Jpn. J. Appl. Phys. **57**, 0902A4 (2018).

[2] M. Lorenz, M. S. R. Rao, T. Venkatesan, E. Fortunato, P. Barquinha, R. Branquinho, D. Salgueiro, R. Martins, E. Carlos, A. Liu *et al.*, The 2016 oxide electronic materials and oxide interfaces roadmap, J. Phys. Appl. Phys. **49**, 433001 (2016).

[3] M. Coll, J. Fontcuberta, M. Althammer, M. Bibes, H. Boschker, A. Calleja, G. Cheng, M. Cuoco, R. Dittmann, B. Dkhil *et al.*, Towards oxide electronics: A roadmap, Appl. Surf. Sci. **482**, 1 (2019).

[4] F. Giustino, J. H. Lee, F. Trier, M. Bibes, S. M. Winter, R. Valentí, Y.-W. Son, L. Taillefer, C. Heil, A. I. Figueroa *et al.*, The 2021 quantum materials roadmap, J. Phys. Mater. **3**, 042006 (2021).

[5] N. A. Spaldin and R. Ramesh, Advances in magnetoelectric multiferroics, Nat. Mater. **18**, 203 (2019).

[6] S. Manipatruni, D. E. Nikonov, C.-C. Lin, T. A. Gosavi, H. Liu, B. Prasad, Y.-L. Huang, E. Bonturim, R. Ramesh, and I. A. Young, Scalable energy-efficient magnetoelectric spin–orbit logic, Nature (London) **565**, 35 (2019).

[7] A. Manchon, J. Zelzny, I. M. Miron, T. Jungwirth, J. Sinova, A. Thiaville, K. Garello, and P. Gambardella, Current-induced spin-orbit torques in ferromagnetic and antiferromagnetic systems, Rev. Mod. Phys. **91**, 035004 (2019).

[8] D. Preziosi, S. Homkar, C. Lefèvre, M. Salluzzo, and N. Viart, Unusual anisotropic magnetic orbital moment obtained from x-ray magnetic circular dichroism in a multiferroic oxide system, Phys. Rev. B **103**, 184420 (2021).

[9] S. Ohkoshi, A. Namai, and S. Sakurai, The origin of ferromagnetism in ε-Fe_2O_3 and ε-$Ga_xFe_{2-x}O_3$ nanomagnets, J. Phys. Chem. C **113**, 11235 (2009).

[10] J. Atanelov and P. Mohn, Electronic and magnetic properties of $GaFeO_3$: *Ab initio* calculations for varying Fe/Ga ratio, inner cationic site disorder, and epitaxial strain, Phys. Rev. B **92**, 104408 (2015).

[11] Y.-C. Tseng, N. M. Souza-Neto, D. Haskel, M. Gich, C. Frontera, A. Roig, M. van Veenendaal, and J. Nogues, Nonzero orbital moment in high coercivity ε-Fe_2O_3 and low-temperature collapse of the magnetocrystalline anisotropy, Phys. Rev. B **79**, 094404 (2009).

[12] M. Gich, A. Roig, C. Frontera, E. Molins, J. Sort, M. Popovici, G. Chouteau, D. Martín y Marero, and J. Nogués, Large coercivity and low-temperature magnetic reorientation in ε-Fe_2O_3 nanoparticles, J. Appl. Phys. **98**, 044307 (2005).

[13] S. Sakurai, J. Jin, K. Hashimoto, and S. Ohkoshi, Reorientation phenomenon in a magnetic phase of ϵ-Fe_2O_3 nanocrystal, J. Phys. Soc. Jpn. **74**, 1946 (2005).

[14] M. Trassin, N. Viart, G. Versini, S. Barre, G. Pourroy, J. Lee, W. Jo, K. Dumesnil, C. Dufour, and S. Robert, Room temperature

ferrimagnetic thin films of the magnetoelectric $Ga_{2-x}Fe_xO_3$, J. Mater. Chem. **19**, 8876 (2009).

[15] C. T. Chen, Y. U. Idzerda, H.-J. Lin, N. V. Smith, G. Meigs, E. Chaban, G. H. Ho, E. Pellegrin, and F. Sette, Experimental Confirmation of the x-Ray Magnetic Circular Dichroism Sum Rules for Iron and Cobalt, Phys. Rev. Lett. **75**, 152 (1995).

[16] B. T. Thole, P. Carra, F. Sette, and G. van der Laan, X-Ray Circular Dichroism as a Probe of Orbital Magnetization, Phys. Rev. Lett. **68**, 1943 (1992).

[17] S. Homkar, D. Preziosi, X. Devaux, C. Bouillet, J. Nordlander, M. Trassin, F. Roulland, C. Lefèvre, G. Versini, S. Barre *et al.*, Ultrathin regime growth of atomically flat multiferroic gallium ferrite films with perpendicular magnetic anisotropy, Phys. Rev. Mater. **3**, 124416 (2019).

[18] F. Polack, M. Silly, C. Chauvet, B. Lagarde, N. Bergeard, M. Izquierdo, O. Chubar, D. Krizmancic, M. Ribbens, J. -P. Duval *et al.*, TEMPO: A new insertion device beamline at SOLEIL for time resolved photoelectron spectroscopy experiments on solids and interfaces, in *SRI 2009, 10th International Conference on Radiation Instrumentation*, AIP Conf. Proc. No. 1234 (AIP, Melville, NY, 2010), p. 185.

[19] R. Nakajima, J. Stohr, and Y. U. Idzerda, Electron-yield saturation effects in *L*-edge x-ray magnetic circular dichroism spectra of Fe, Co, and Ni, Phys. Rev. B **59**, 6421 (1999).

[20] See Supplemental Material at http://link.aps.org/supplemental/10.1103/PhysRevB.106.184410 for further details on simulations of the XAS spectra, thickness dependence of the XMCD data, RESPES experiments, and cationic site occupancies.

[21] R. Jones, R. Nickel, P. K. Manna, J. Himan, and J. van Lierop, Temperature and field evolution of site-dependent magnetism in ε-Fe_2O_3 nanoparticles, Phys. Rev. B **100**, 094425 (2019).

[22] J. Stöhr, Exploring the microscopic origin of magnetic anisotropies with x-ray magnetic circular dichroism (XMCD) spectroscopy, J. Magn. Magn. Mater. **200**, 470 (1999).

[23] C. Lefevre, F. Roulland, A. Thomasson, C. Meny, F. Porcher, G. Andre, and N. Viart, Magnetic and polar properties' optimization in the magnetoelectric $Ga_{2-x}Fe_xO_3$ compounds, J. Phys. Chem. C **117**, 14832 (2013).

[24] J. Zhang, R. Skomski, Y. F. Lu, and D. J. Sellmyer, Temperature-dependent orbital moment anisotropy in dilute magnetic oxides, Phys. Rev. B **75**, 214417 (2007).

[25] J. Y. Kim, T. Y. Koo, and J. H. Park, Orbital and Bonding Anisotropy in a Half-Filled $GaFeO_3$ Magnetoelectric Ferrimagnet, Phys. Rev. Lett. **96**, 047205 (2006).

[26] T. Arima, D. Higashiyama, Y. Kaneko, J. P. He, T. Goto, S. Miyasaka, T. Kimura, K. Oikawa, T. Kamiyama, R. Kumai *et al.*, Structural and magnetoelectric properties of $Ga_{2-x}Fe_xO_3$ single crystals grown by a floating-zone method, Phys. Rev. B **70**, 064426 (2004).

[27] B. T. Thole and G. van der Laan, Branching ratio in x-ray absorption spectroscopy, Phys. Rev. B **38**, 3158 (1988).

[28] B. T. Thole and G. van der Laan, Linear relation between x-ray absorption branching ratio and valence-band spin-orbit expectation value, Phys. Rev. A **38**, 1943 (1988).

[29] M. Haverkort, Spin and orbital degrees of freedom in transition metal oxides and oxide thin films studied by soft x-ray absorption spectroscopy, Ph.D. thesis, Universität zu Köln, 2005.

[30] J. Honolka, S. Krotzky, M. Herzog, T. Herden, V. Sessi, H. Ebert, J. Minár, K. von Bergmann, R. Wiesendanger, and O. Šipr, Spin-spiral state of a Mn monolayer on W(110) studied by soft x-ray absorption spectroscopy at variable temperature, Phys. Rev. B **103**, 174419 (2021).

[31] D. Alders, L. H. Tjeng, F. C. Voogt, T. Hibma, G. A. Swatzky, C. T. Chen, J. Vogel, M. Sacchi, and S. Iacobucci, Temperature and thickness dependence of magnetic moments in NiO epitaxial films, Phys. Rev. B **57**, 11623 (1998).

[32] D. Schmitz, C. Schmitz-Antoniak, A. Warland, M. Darbandi, S. Haldar, S. Bhandary, O. Eriksson, B. Sanyal, and H. Wende, The dipole moment of the spin density as a local indicator for phase transitions, Sci. Rep. **4**, 5760 (2014).

[33] S. Homkar, E. Martin, B. Meunier, A. Anadon-Barcelona, C. Bouillet, J. Gorchon, K. Dumesnil, C. Lefèvre, F. Roulland, O. Copie *et al.*, Spin current transport in hybrid Pt/multifunctional magnetoelectric $Ga_{0.6}Fe_{1.4}O_3$ bilayers, ACS Appl. Electron. Mater. **3**, 4433 (2021).

[34] E. Verwey, Electronic conduction of magnetite Fe_3O_4 and its transition point at low temperatures, Nature (London) **144**, 327 (1939).

[35] F. Walz, The Verwey transition—a topical review, J. Phys.: Condens. Matter **14**, R285 (2002).

[36] A. R. Muxworthy and E. McClelland, Review of the low-temperature magnetic properties of magnetite from a rock magnetic perspective, Geophys. J. Int. **140**, 101 (2000).

[37] M. Imada, A. Fujimori, and Y. Tokura, Metal-insulator transitions, Rev. Mod. Phys. **70**, 1039 (1998).

[38] M. S. Senn, J. P. Wright, and J. P. Attfield, Charge order and three-site distortions in the Verwey structure of magnetite, Nature (London) **481**, 173 (2012).

[39] J. P. Attfield, Magnetism and the trimeron bond, Chem. Mater. **34**, 2877 (2022).

[40] M. G. Silly, F. Charra, F. Lux, G. Lemercier, and F. Sirotti, The electronic properties of mixed valence hydrated europium chloride thin film, Phys. Chem. Chem. Phys. **17**, 18403 (2015).

[41] J. Szade, W. Burian, Z. Celiński, T. O'Keevan, M. Zangrando, F. Bondino, and E. Magnano, Resonance induced divalent Eu states in EuF_3 ultrathin layer, Surf. Sci. **580**, 163 (2005).

[42] J. Chen, D. Huang, A. Tanaka, C. Chang, S. Chung, W. Wu, and C. Chen, Magnetic circular dichroism in Fe 2*p* resonant photoemission of magnetite, Phys. Rev. B **69**, 085107 (2004).

[43] M. Hoesch, P. Piekarz, A. Bosak, M. Le Tacon, M. Krisch, A. Kozlowski, A. M. Oleś, and K. Parlinski, Anharmonicity Due to Electron-Phonon Coupling in Magnetite, Phys. Rev. Lett. **110**, 207204 (2013).

[44] S. Mukherjee, A. Garg, and R. Gupta, Spin glass-like phase below similar to 210 K in magnetoelectric gallium ferrite, Appl. Phys. Lett. **100**, 112904 (2012).